JOURNAL OF PROPULSION AND POWER
Vol. 17, No. 2, March–April 2001

Combustion Efficiencies of Supersonic Flames

Albert Ratner* and James F. Driscoll†
University of Michigan, Ann Arbor, Michigan 48109-2118
Hwanil Huh‡
Chungnam National University, Taejon 305-764, Republic of Korea
and
Rodney A. Bryant§
National Institute of Science and Technology, Gaithersburg, Maryland 20899

Measured values of combustion efficiency η_c, which quantify the amount of hydrogen fuel that remains unburned because the fuel has insufficient residence time in the reaction zone of a supersonic flame, are reported. Trends are reported as the fuel flow rate and the stagnation temperature are systematically varied. The combustion efficiency measurements are needed to assess chemistry submodels of numerical simulations of supersonic flames. A hydrogen jet flame is stabilized on the axis of a Mach 2.5 wind tunnel, and to explain why some fuel remains unburned images were obtained of the fuel concentration and the OH radical concentration using planar laser-induced fluorescence. Increasing the fuel flow rate (and overall fuel-air equivalence ratio from 0.034 to 0.068) is found to increase the combustion efficiency and the flame length. It is believed that the increased residence time of fuel in the longer flames causes the observed increase in efficiency. The increase the combustion efficiency caused by an increase in the stagnation temperature is quantified. Oblique shock waves were added and were found to decrease combustion efficiency if the waves are positioned to create a radial outflow of fuel away from the OH radical zone, which reduces the residence time.

Nomenclature

c	=	calibration constant
M_c	=	convective Mach number
$\dot{m}$	=	mass-flow rate
X	=	mole fraction
Y	=	mass fraction
η_c	=	combustion efficiency, defined in Eq. (1)
ϕ	=	overall fuel-air equivalence ratio

Introduction

THE goal of this research is to measure certain parameters within a simple supersonic jet flame, which can provide a sensitive assessment of new models of supersonic combustion. Previously a hydrogen jet flame was stabilized along the centerline of a Mach 2.5 wind tunnel, and measurements were made of the flame lengths,[1] the blowout limits,[2,3] and wall pressures.[4,5] Recently, Roy and Edwards[6] reported some results of their hybrid k–ω/k–ε numerical simulation of the present experiment; they simulated the present geometry with a $129 \times 153 \times 49$ grid, and for their inlet boundary conditions they used measured values of flow properties that are found in Refs. 1–5. Roy and Edwards[6] were able to simulate accurately the shock/expansion wave pattern and wall pressures of the present experiment.

The present paper reports a systematic set of measurements of the combustion efficiencies of supersonic flames, which quantifies the amount of hydrogen fuel that remains unburned because it has insufficient residence time in the reaction zone. Previously, only a few measurements of the combustion efficiency of supersonic flames have been reported in the archival literature.[7–9] Supersonic flames involve complex interactions between large fluid-mechanical shearing rates and short residence times during which the chemistry is incomplete. For example, Roy and Edwards[6] simulated the present supersonic flame using a 9-species, 21-reaction hydrogen oxidation mechanism, but they have not yet reported values of combustion efficiency. Other chemistry schemes are employed by the supersonic flame models of Eklund et al.,[10] Villasenor et al.,[11] Zheng and Bray,[12] and Baurle et al.[13]

Combustion efficiency η_c is defined by Heiser and Pratt[14] (p. 331) as

$$\eta_c = \frac{\dot{m}_{\mathrm{H2,Burned}}}{\dot{m}_{\mathrm{H2,Total}}} = 1 - \frac{\dot{m}_{\mathrm{H2,unburned}}}{\dot{m}_{\mathrm{H2,Total}}} \tag{1}$$

which is the mass-flow rate of hydrogen that burns $\dot{m}_{\mathrm{H2,Burned}}$ divided by the total mass-flow rate of hydrogen $\dot{m}_{\mathrm{H2,Total}}$. Equation (1) can be recast as

$$\eta_c = 1 - \frac{Y_{\mathrm{H2,unburned}}}{Y_{\mathrm{H2,initial}}} \tag{2}$$

$Y_{\mathrm{H2,unburned}}$ is the mass fraction of unburned hydrogen that is measured with a sampling probe far downstream of the flame, and $Y_{\mathrm{H2,initial}}$ is the known ratio of the injected hydrogen mass-flow rate to the total incoming mass-flow rates of hydrogen and air at the fuel injector ($x = 0$). Other studies[7–9] have used the same definition of combustion efficiency as is given by Eq. (2). Heiser and Pratt[14] also describe a second way to define combustion efficiency, which is the enthalpy that is liberated by combustion divided by the enthalpy of combustion that is available; this second definition was not used because temperature was not measured.

The purpose of the present work was not to simulate actual scramjet conditions, but to study a supersonic jet flame which is of sufficiently simple geometry such that it can be simulated using current models. Stagnation temperatures and fuel flow rates of the present experiment are described next and are much less than values associated with actual scramjets. However the present conditions allow flow visualization diagnostics to be used. Other studies of laboratory-scale supersonic flames have been reported by Cheng et al.,[15] Segal et al.,[16] and Barlow et al.[17]

Received 21 January 2000; accepted for publication 11 June 2000.

*Francois Xavier Bagnoud Fellow, Department of Aerospace Engineering, Building 2118. Member AIAA.
†Professor, Department of Aerospace Engineering, Building 2118. Associate Fellow AIAA.
‡Assistant Professor, Department of Aerospace Engineering. Member AIAA.
§Research Scientist, 100 Bureau Drive, Mail Stop 8653. Member AIAA.

Experimental Arrangement

A schematic of the experiment is shown in Figs. 1a and 1b; additional dimensions and details are reported in Refs. 1–5. Hydrogen fuel is injected along the centerline of a Mach 2.5 wind tunnel, as shown in Fig. 1a. The wind tunnel shown in Fig. 1b consists of a compressed air supply, a 250-kW electrical air heater, a settling chamber, a Mach 2.5 converging-diverging nozzle, a rectangular test section with four quartz optical windows, and a water-cooled diffuser. The rectangular test section is 55.3 cm long, and two of the sidewalls diverge at an angle of 4 deg, as shown in Fig. 1a, to maintain a uniform Mach number as heat is added to the flow. The location $x = 0$ is the upstream boundary of the test where the fuel is injected; at $x = 0$ the wind-tunnel dimensions are 5.77×4.06 cm. The fuel injector is a circular tube that has an outer diameter of 2.54 cm and an inner diameter of 0.64 cm. The fuel and airflow rates were measured using calibrated choked orifices and calibrated pressure gauges. The test section has a rectangular cross section because of the need for flat windows for laser diagnostics. The fuel injector is a circular thick-lipped tube on the centerline; the fuel injector was chosen to be an axisymmetric tube, rather than a two-dimensional-slot, in order to avoid flame interaction with sidewalls.

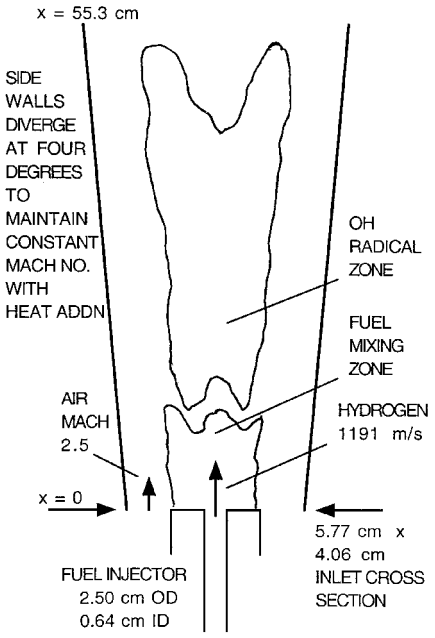

Fig. 1a Schematic of the University of Michigan supersonic combustor test section. Boundary conditions at $x = 0$ are listed in Table 1; hydrogen fuel = fully developed pipe flow, supersonic air velocity profiles (see Ref. 5).

Table 1 is a list of the inlet boundary conditions, including the fuel velocity, air velocity, fuel density, and air density at the fuel injection plane ($x = 0$). The velocity profile in the airstream at $x = 0$ was determined from pitot probe surveys.[5] The velocity profile of the hydrogen stream at $x = 0$ was not measured, but can be assumed to be identical to the profile for fully developed pipe flow that is given in Hinze[18] because the length of the hydrogen injector tube is 60 times its inner diameter. The hydrogen is frictionally choked in the fuel tube so that the fuel-tube exit Mach number is unity. The convective Mach number M_c was computed to be 0.30 at the fuel injection plane ($x = 0$) for condition 1 listed in Table 1. Papamoschou and Roshko[19] showed that M_c is $(U_1 - U_c)/a_1$, where the convective velocity U_c is $(U_1 a_2 + U_2 a_1)/(a_1 + a_2)$. At the injector plane for condition 1, the fuel velocity U_1 is 1191 m/s, the air velocity U_2 is 745 m/s, and the speed of sound a_1 is 1191 m/s while a_2 is 299 m/s. M_c decreases in the downstream direction because the air Mach number remains constant but the velocity in the fuel jet decreases so that M_c is everywhere less than 0.3. Reference 19 indicates that for the present values of convective Mach number the effects of compressibility on the mixing are negligible. The supersonic flame has the appearance of a jet flame, but the flame base is lifted about

Table 1 Boundary conditions at the fuel-injection plane ($x = 0$) for three supersonic flames

Case number	1[a]	2[b]	3[c]
Fuel mass flow m_F, g/s	0.8	1.6	1.6
Air stagnation temperature T_{0A}, K	500	500	284
Air Mach number M_A	2.5	2.5	2.5
Air velocity U_A, m/s	745	745	561
Air stagnation pressure p_{0A}, atm	6.44	6.44	6.44
Air static pressure p_A, atm	0.38	0.38	0.38
Air mass flow m_A, kg/s	0.80	0.80	1.06
Air static temperature T_A, K	222	222	126
Overall equiv. ratio ϕ	0.034	0.068	0.052
Fuel stagnation pressure p_F, atm	2.5	5.0	5.0
Fuel velocity U_F, m/s	1191	1191	1191
Fuel Mach number M_F	1.0	1.0	1.0
Fuel Reynolds number $U_F\, d/\nu_F$	76,000	152,000	152,000
Convective Mach number M_c	0.30	0.30	0.45

[a] 1 = baseline.
[b] 2 = increased fuel flow rate.
[c] 3 = lower stagnation temperature T_{0A}.

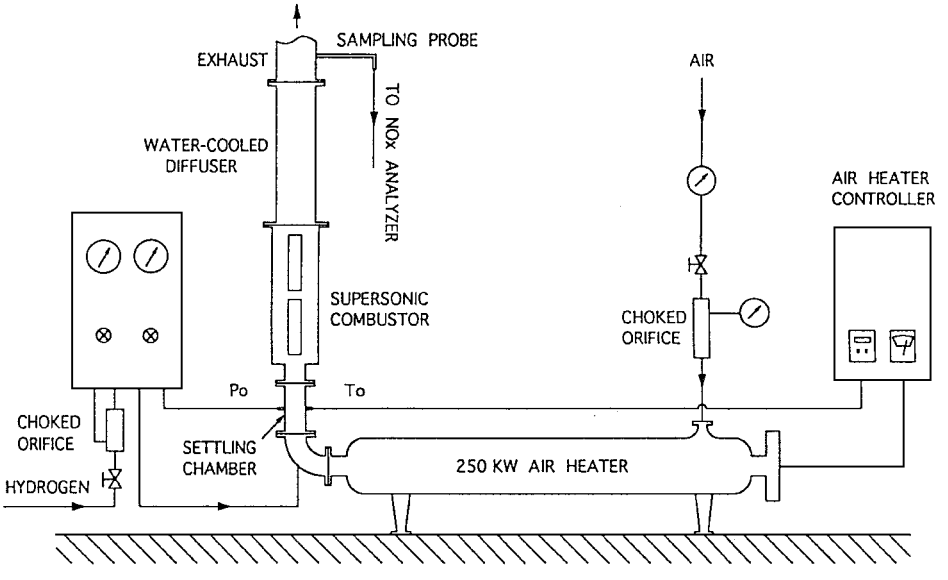

Fig. 1b Schematic of air heater, choked orifice flowmeters, settling chamber, and sampling probe.

5 cm above the fuel tube. The fuel tube acts as a bluff body that creates a recirculation zone of subsonic velocities in which the flame base stabilizes. The visible flame length varies from 12 to 25 cm as the fuel flow rate is increased.[1]

Combustion efficiency is defined by Eq. (2) and was determined by measuring the mass fraction of unburned hydrogen fuel using a gas sampling probe that has an inner diameter of 1.3 mm. The probe was mounted on the centerline 2 m downstream of the combustor. The hydraulic diameter of the test section is 7 cm, and so the probe is located 28 hydraulic diameters downstream of the combustor. The product gases are well mixed at this downstream probe location, as has been shown in previous studies with sampling probes.[20] In Ref. 20 the sample probe was traversed radially across the exhaust duct from one wall to the other wall, and no significant change in the probe reading occurred. The present experiment is operated at a higher Reynolds number and with a probe that was farther downstream than in Ref. 20 so that the exhaust gases are well mixed.

The sensor is a Toximet Series Hydrogen Detector, manufactured by Enmet Corporation, and its operation is based on the catalytic principle. Hydrogen bonds to the sensor surface, causing a change in its electrical resistance. The detector requires 1–1.5 min to yield a steady reading. The sensor reading is denoted $\chi_{H2,sensor}$, and this mole fraction is related to the mass fraction of unburned hydrogen by

$$\chi_{H2,sensor} = c_1 Y_{H2,unburned} \tag{3}$$

The quantity c_1 is described in the Appendix; it depends on the standard relation between mole fraction and mass fraction, as well as a standard (small) correction of 3–6% that is required because the sensor reading is a dry reading because water vapor must be removed from the sampling line. The relation for combustion efficiency is obtained by combining Eqs. (2) and (3) to yield

$$\eta_c = 1 - \left\{ \frac{(\chi_{H2,sensor}/c_1)}{[\dot{m}_{H2,in}/(\dot{m}_{AIR,in} + \dot{m}_{H2,in})]} \right\} \tag{4}$$

Combustion efficiency was determined by using Eq. (4) and the sensor reading $\chi_{H2,sensor}$. The calibration constant c_1 is described in the Appendix, and the fuel and air mass-flow rates ($\dot{m}_{H2,in}$, $\dot{m}_{AIR,in}$) were measured using flow meters. An uncertainty analysis for the measurement technique is given in the Appendix.

To image the fuel mixing zone, acetone was added to the hydrogen fuel in trace amounts; the acetone mole fraction was 0.0072 and 0.0058 for the 1.4 and 0.95 g/s fuel mass-flow rates, respectively. A fraction of the total hydrogen flow was bubbled through liquid acetone. It was verified that the acetone mole fraction in this stream of hydrogen was approximately the known saturation mole fraction because the acetone mole fraction [as monitored by the planar laser-induced fluorescence (PLIF) system] did not change with the residence time of the gas in the acetone chamber. The use of acetone as a flow tracer is described by Lozano et al.,[21] Grisch et al.,[22] and Bryant et al.[23] Acetone fluorescence was excited using a Spectra-Physics GCR-250 Nd-YAG laser operated at a wavelength of 266 nm.

Images of the OH concentration field were obtained by tuning the output of a Lumonics HD 300 Nd:YAG-pumped dye laser to 282.75 nm to excite the $Q_1(5)$ line of the (1, 0) band of the $A^2\Sigma \leftarrow X^2\Pi$ transition of the OH molecule. A cooled, slow-scan, intensified charge-coupled device array camera (Princeton Instruments ICCD 576) was used to image a field of view of 5.3 × 8 cm; the laser light sheet thickness was 0.3 mm.

Results

Sources of Combustion Inefficiency

The sources of combustion efficiency are better understood by considering Fig. 2, which is a set of PLIF images of the fuel-air mixing zone and the OH radical zone in the supersonic flame. It is seen that Fig. 2 consists of five images; each image was taken at a different time but the images are positioned to indicate the overall

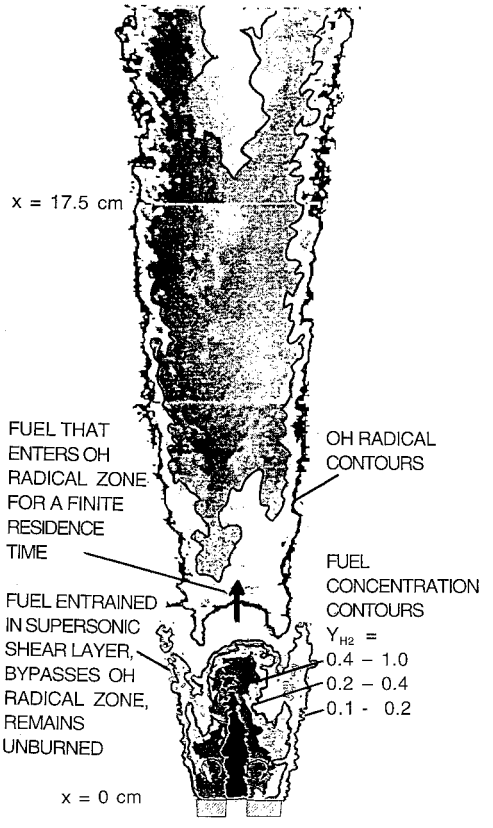

Fig. 2 Measured images of the OH reaction zone and the fuel mixing zone in the supersonic flame, using PLIF.

structure of the supersonic flame. The lowest image indicates the contours of the hydrogen fuel mass fraction, which are proportional to the contours of the fluorescence from the acetone that was seeded into the hydrogen. The upper four images in Fig. 2 show the OH fluorescence contours.

Figure 2 shows that three physical processes occur: 1) the supersonic flame is lifted by 5 cm above the fuel injector and that much of the fuel-air mixing takes place upstream of the flame base, 2) the centerline region appears to have the structure of a fuel-rich premixed flame because fuel-rich conditions occur just upstream of the OH reaction zone, and 3) peninsulas of fuel appear at each side of the fuel mixing zone; these peninsulas are caused by the shear layer associated with the supersonic airstream, which entrains fuel and convects it downstream.

Based on the images shown in Fig. 2, it is believed that there are two major sources of combustion inefficiency: insufficient residence time to burn the fuel that enters the OH radical zone and the bypass of fuel around the OH radical zone as a result of the supersonic shear layer. This fuel bypass phenomenon is believed to be a general property of supersonic flames because nearly all supersonic flames reported in the literature,[1–6, 15–17] including all flames studied in our laboratory, are lifted to some degree. It is usually not possible for a supersonic flame base to remain attached to a fuel injector, whether it be an axial fuel injector or a sidewall fuel injector into a transverse flow. It is not possible to see the fuel actually bypass the OH radical zone in Fig. 2 because fuel concentrations just upstream of the OH radical zone are too small to be imaged with current diagnostics. The supersonic shear layer rapidly mixes some of the fuel to a concentration of typically 4000 ppm, which is no longer flammable and is no longer detectable with imaging diagnostics.

For comparison purposes Fig. 3 shows the computed images of the OH radical zone and the fuel mixing zone that were reported by Roy and Edwards[6] for the present geometry, flow rates, and inlet profiles. Figure 3 shows that the Roy and Edwards[6] simulation correctly predicts that the flame is lifted by about 5 cm, that the OH radical zone is separate and downstream of the fuel mixing zone, and that

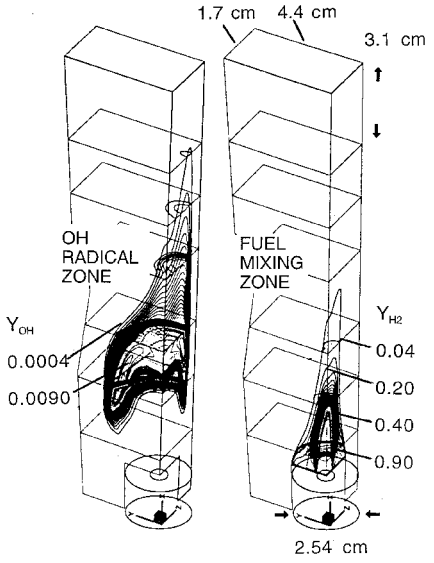

Fig. 3 OH radical zone and the fuel mixing zone computed by Roy and Edwards[6] for the exact geometry and fuel/air boundary conditions as the present experiment. Computation uses Menter's hybid $k-\varepsilon$ model with 9 species, 21 reaction hydrogen chemistry.

the model approximately predicts the measured length of the fuel mixing zone. The length of the OH radical zone is somewhat underpredicted, and some other features are not predicted accurately for reasons that require additional research. However, because both the experimental images and numerical model of the supersonic flame have only recently been made available, the general agreement is encouraging. Roy and Edwards[6] do not report any computed values of combustion efficiency.

Effect of Varying Fuel Mass Flow and Stagnation Temperature on Combustion Efficiency

Figure 4 illustrates how the combustion efficiency of the supersonic flame varies as the fuel mass-flow rates and stagnation temperatures are varied. Although the relatively low stagnation temperatures of 500 and 284 K are not intended to represent propulsion conditions, they were chosen because they provide a fairly wide range of combustion efficiencies, which are a good test of numerical models; it is seen that η_c varies from 0.70 to 0.88 in Fig. 4.

Increasing the fuel flow rate is seen to cause an increase in the values of η_c in Fig. 4, which is believed to be a result of several reasons. First, the flame becomes wider and has an increased volume as the fuel flow rate increases; the flame occupies a larger fraction of the wind-tunnel cross-sectional area so that it is less likely that fuel can be convected around the flame and remain unburned. Second, the flame region near the centerline is expected to be similar to a rich premixed flame, based on the physical image presented in Fig. 2. It is believed that some fuel passes through the rich premixed flame near the centerline and enters the OH radical zone, but not all of this fuel can be oxidized because of the limited residence times at supersonic conditions. Increasing the fuel flow rate causes a large increase in the flame length, as reported by Driscoll et al.,[1] and the longer flames provide a longer residence time for fuel oxidation. In addition, the fuel in the supersonic shear layer can be preheated as it is convected near the upstream boundary of the OH radical zone in Fig. 2; larger fuel flow rates create flames having larger volume, which would be expected to preheat the nearby fuel more effectively, and reduce the possibility that the fuel-air mixture can escape the heating process.

Increasing the stagnation temperature from 284 to 500 K is seen to cause an increase in the combustion efficiency, as expected. The data in Fig. 4 quantify the sensitivity of the combustion efficiency to stagnation temperature; a reasonable two-parameter empirical fit to the temperature sensitivity of Fig. 4 is

$$\eta_c = [A \exp(E/RT_0) + 1]^{-1} \tag{5}$$

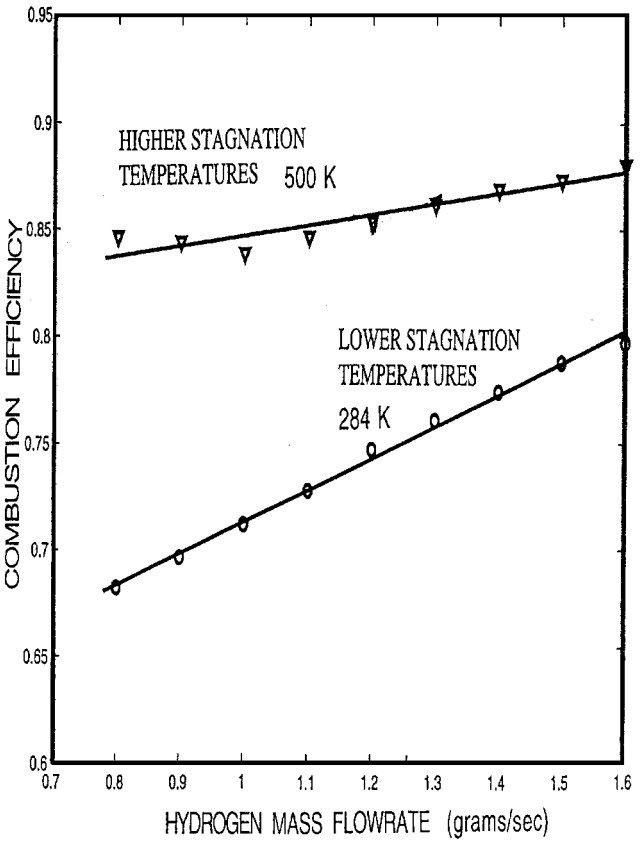

Fig. 4 Measured combustion efficiencies η_c for the supersonic flames for various fuel flow rates and two different stagnation temperatures. Combustion efficiency defined by Eq. (1). For these cases no wedges on the sidewall were used to create shock waves.

where A has the value 0.0483 and is proportional to the ratio of a characteristic chemical reaction time to the residence time, and E is 1.28 kcal/mole for the baseline fuel flow rate of 0.8 g/s; the universal gas constant R is 1.987 cal/mole-K. Properly predicting the measured sensitivity to temperature given by Eq. (5) represents a challenge for future supersonic flame chemistry codes.

Effects of Shock Waves on Combustion Efficiency

Because our previous work[3] has shown that introducing shock waves causes a significant effect on flame properties (such as flame blowout limits), the effect of shock waves on combustion efficiency was measured. Photographs in Figs. 5c and 5d show the wedges that were mounted on the sidewalls at $x = 2.8$ cm; these photographs were previously reported by Huh and Driscoll[3] and are presented to document the shock-wave locations. The wedges have a slope of 10 deg and extended 6 mm from the wall and were mounted at either $x = 2.8$ cm or at 5.95 cm.

Figure 6 shows that the shock waves do have a significant effect, and, in general, they reduce the combustion efficiency by a significant amount (from 85 to 75%). Shock waves have two major effects: they raise the static temperature of the gas, and they produce a turning of the flow, which can create radial inflow or radial outflow, depending on the shock location, which affects the width and length of the OH reaction zone.

Figure 5 proves that the shock waves clearly make the flame narrower because the maximum diameter of the flame in Fig. 5c is less than that of Fig. 5a. Similarly the flame diameter in Fig. 5d is less than in Fig. 5b. This is expected because the shock waves turn the flow toward the centerline; in fact the flame diameter in Figs. 5c and 5d is decreasing in the downstream direction, forming a visible "neck" in the flame caused by the shock waves. The shock waves also cause a "splitting" of the flame seen in Fig. 5c; the flame appears to be locally extinguished near the tip, and several bright regions

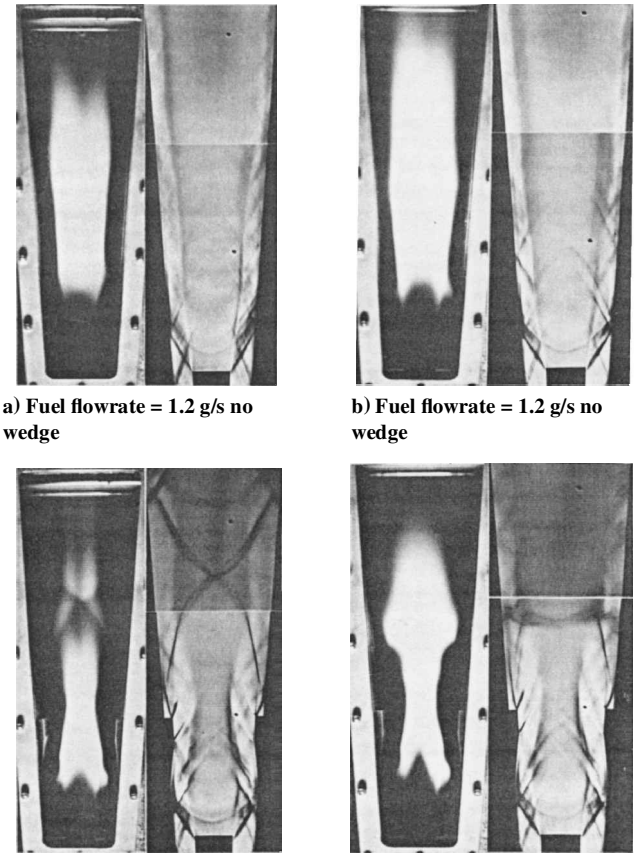

a) Fuel flowrate = 1.2 g/s no wedge

b) Fuel flowrate = 1.2 g/s no wedge

c) Fuel flowrate = 1.2 g/s 10 deg wedge

d) Fuel flowrate = 1.6 g/s 10 deg wedge

Fig. 5 Direct photographs and schlieren photographs of the supersonic flames; top row: no wedges on sidewalls to create shock waves; bottom row: wedges on sidewalls were used to create the shock waves shown. T_0 = 284 K.

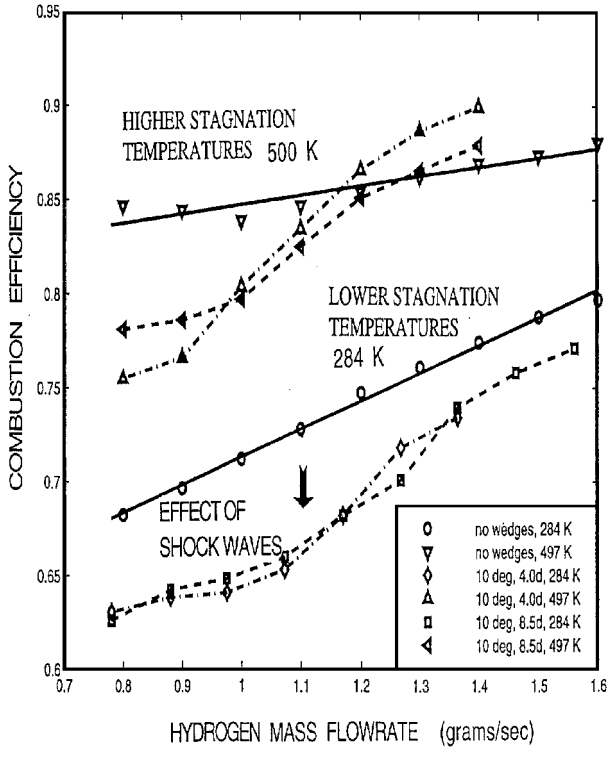

Fig. 6 Effect of shock waves on the combustion efficiency η_c of supersonic flames. In some cases shocks reduce the combustion efficiency by diverting fuel away from the OH radical zone, whereas in some cases shocks increase efficiency by diverting fuel toward OH radical zone.

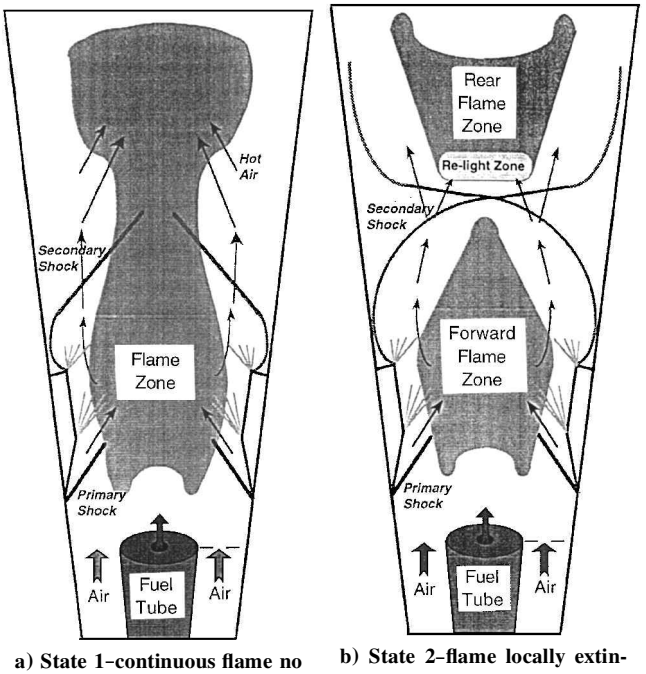

a) State 1–continuous flame no local extinction

b) State 2–flame locally extinguished by shocks

Fig. 7 Different observed states of the supersonic flame caused by shock waves impinging on the flame, showing how the combustion efficiency is affected.

are separated by dark zones. The dark regions of local extinction are believed to be a result of the radial inflow of cold air caused by the shocks.

The reduction in combustion efficiency caused by shock waves that is reported in Fig. 6 is believed to be a result of both the observed narrowing of the flame and the observed zones of flame extinction. A narrow flame can allow more fuel to convect around the OH radical zone and remain unburned. The observed regions of flame extinction also can allow fuel to remain unburned.

The flame can be considered to be in one of two possible states, as shown by Fig. 7, which is a schematic drawing of the photographs in Fig. 5. State 1 is a continuous flame having no observed dark zones (i.e., no local flame extinction); state 2 is a locally extinguished flame, which has the dark zones seen in Fig. 5 where the shock waves extinguish the flame. In state 2 there is enough fuel flow rate so that the flame relights downstream of the shock-wave region. While the primary shock waves narrow the flame and cause radial inflow of air, one also sees a series of reflected shocks that widen the flame downstream of the neck region. The large x-shaped shocks in Figs. 5c and 7b represent a secondary recompression shock and its reflection. To correctly model supersonic flames and their combustion efficiency, especially if shock waves exist, it is important that the general shape and structure of the flames (as shown in Figs. 2, 5, and 7) be known and modeled correctly.

Conclusions

1) The combustion efficiencies of supersonic hydrogen-air flames of simple geometry have been quantified for 50 different run conditions in order to deduce general trends that can be numerically simulated. Combustion efficiency is a parameter that provides a sensitive test of the chemistry and mixing submodels of supersonic flame models.

2) As the fuel flow rate is increased, the combustion efficiency increases linearly. This is believed to be a result of an increase in the flame width, which prevents fuel from passing around the OH radical zone, and an increase in flame length, which increases the residence time of fuel in the OH radical zone.

3) The sensitivity of the combustion efficiency to increases in the stagnation temperature was quantified; results are represented by Eq. (5). Proper simulation of this measured temperature sensitivity

can provide an assessment of the chemical kinetics submodels used to simulate supersonic flames.

4) Images of the fuel mixing zone and the OH radical zone in the supersonic flame are presented in the attempt to understand where the fuel mixes and how it could escape the combustion region. However, the sources of the combustion inefficiencies require further research.

5) Adding shock waves causes a significant decrease in the combustion efficiency of the present flames; shock waves cause the flames to become narrower and form a "neck," which is believed to allow more fuel to convect past the OH radical zone and remain unburned.

Appendix: Hydrogen Sensor Calibration and Uncertainty Analysis

Calibration of the hydrogen sensor requires that the quantity c_1 in Eq. (3) of the main text be experimentally determined:

$$\chi_{\mathrm{H2,sensor}} = c_1 Y_{\mathrm{H2,unburned}} \tag{3}$$

A common problem associated with sampling techniques is that the detector reading has to be corrected by a few percent because after combustion some of the water that is generated condenses out on the wall of the wind-tunnel cooling section or in the sampling probe. Therefore, a standard procedure was used, which utilized an ice bath to remove all the water vapor, and thus $\chi_{\mathrm{H2,sensor}}$ is a dry measurement of the hydrogen mole fraction. A small correction to the dry measurement must be made to obtain the actual hydrogen mole fraction, which is $\chi_{\mathrm{H2,unburned}}$, thus

$$\chi_{\mathrm{H2,sensor}} = c_2 \chi_{\mathrm{H2,unburned}} \tag{A1}$$

The relation between hydrogen mass fraction and mole fraction is

$$\chi_{\mathrm{H2,unburned}} = c_3 Y_{\mathrm{H2,unburned}} \tag{A2}$$

and it follows from Eqs. (3), (A1), and (A2) that

$$c_1 = c_2 \cdot c_3 \tag{A3}$$

To obtain the functions c_1, c_2, and c_3, consider the case for which one mole of hydrogen is consumed and a moles of hydrogen remain unburned. Then $(1+a)$ moles of hydrogen will form one mole of water vapor and a moles of unburned hydrogen, as given by

$$(1+a)\mathrm{H_2} + (1/2\phi)\mathrm{O_2} + (1/2\phi)\left(\tfrac{79}{21}\right)\mathrm{N_2} \Rightarrow a\mathrm{H_2} + \mathrm{H_2O} + \left(1/2\phi - \tfrac{1}{2}\right)\mathrm{O_2} + (1/2\phi)\left(\tfrac{79}{21}\right)\mathrm{N_2} \tag{A4}$$

ϕ is the known overall equivalence ratio, which is the mass-flow rate of fuel injected divided by the mass-flow rate of air, normalized by the stoichiometric fuel-air ratio. The dry mole fraction of unburned hydrogen is the ratio of a moles of hydrogen to the number of moles on the right side of Eq. (A4), excluding the water vapor:

$$\chi_{\mathrm{H2,sensor}} = a/[a + 0.5\phi^{-1} - 0.5 + 1.88\phi^{-1}] \tag{A5}$$

while the actual wet value of the mole fraction of unburned hydrogen is the ratio of a moles to the total moles on the right side of Eq. (A4), including the water vapor:

$$\chi_{\mathrm{H2,unburned}} = a/[a + 1 + 0.5\phi^{-1} - 0.5 + 1.88\phi^{-1}] \tag{A6}$$

The quantity a is determined by solving Eq. (A5) for a because both $\chi_{\mathrm{H2,sensor}}$ and ϕ are known:

$$a = (2.38 - 0.5\phi)\chi_{\mathrm{H2,sensor}} \tag{A7}$$

Combining Eqs. (A1) and (A5–A7) yields

$$c_2 = 1 + \frac{\phi(1 - \chi_{\mathrm{H2,sensor}})}{(2.38 - 0.5\phi)} \tag{A8}$$

The mass fraction of unburned hydrogen is the molecular weight of hydrogen (2.016 g/mole) multiplied by a moles and divided by the mass of the quantities on the right side of Eq. (A4), thus

$$Y_{\mathrm{H2,unburned}} = \frac{(2.38 - 0.5\phi)[\chi_{\mathrm{H2,sensor}}/(1-\chi_{\mathrm{H2,sensor}})]}{(2.38 - 0.5\phi)[\chi_{\mathrm{H2,sensor}}/(1-\chi_{\mathrm{H2,sensor}})] + \phi + 34.33} \tag{A9}$$

The quantity c_3 is determined from Eqs. (A3), (A6), (A7), and (A9) to be

$$c_3 = \frac{14.42 + 0.42\phi + (1 - 0.21\phi)[\chi_{\mathrm{H2,sensor}}/(1 - \chi_{\mathrm{H2,sensor}})]}{1.0 + 0.21\phi + (1 - 0.21\phi)[\chi_{\mathrm{H2,sensor}}/(1 - \chi_{\mathrm{H2,sensor}})]} \tag{A10}$$

The resulting value of c_1 that is required in Eq. (3) is obtained from Eqs. (A3), (A8), and (A10). The Table lists a typical sensor reading and the values of quantities used to determine the combustion efficiency.

The sensor is temperature compensated, and both temperature and hydrogen gas calibrations are performed by the manufacturer. An additional calibration was performed in the present facility; known amounts of fuel and air were mixed in the wind tunnel and then sampled. The detector has good repeatability and linearity over the range from 200 to 20,000 ppm of H_2, as shown by Fig. A1. The uncertainty in measuring the unburned hydrogen mass fraction $Y_{\mathrm{H2,unburned}}$ caused by the detector is 2%. The uncertainty in measuring the initial mass fraction of hydrogen in the hydrogen and air

Table Typical reading of the hydrogen sensor and the resulting mass fraction of unburned hydrogen

Quantity	Value
Sensor reading ($\chi_{\mathrm{H2,sensor}}$)	2240 ppm
Overall equiv. ratio ϕ	0.034
c_2 [Eq. (A8)]	1.014
Correction for dry reading $(1 - c_2)$	1.4%
c_3 [Eq. (A10)]	14.33
c_1 [Eq. (A3)]	14.53
$[\dot{m}_{\mathrm{H2,in}}/(\dot{m}_{\mathrm{AIR,in}} + \dot{m}_{\mathrm{H2,in}})]$	9.85×10^{-4}
η_c [Eq. (4)]	0.84

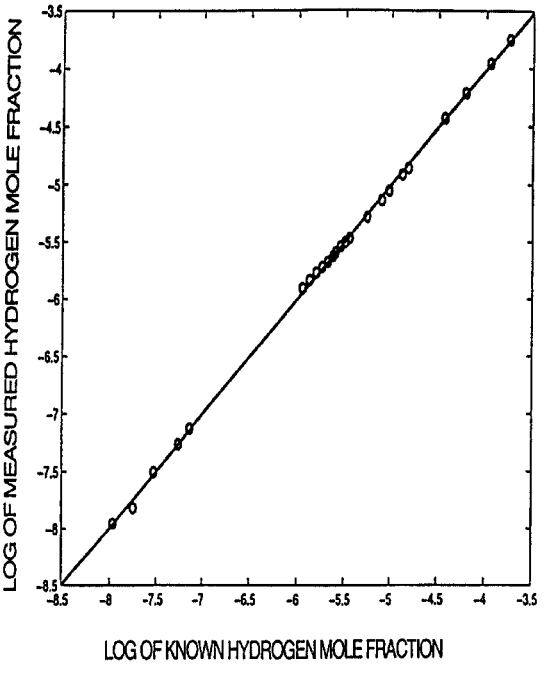

Fig. A1 Calibration of the hydrogen detector. The horizontal axis is the known hydrogen mole fraction (logarithmic units), and the vertical axis is the detector reading. No flame present.

inlet streams ($Y_{H2,initial}$) was 2%, which is caused by uncertainties associated with reading the pressure gauges for the choked orifice flow meters. Therefore the resulting uncertainty in the combustion efficiency determined from Eq. (2) is the square root of the sum of $(0.02)^2$ and $(0.02)^2$, which is 3%.

Acknowledgments

Support for Albert Ratner was made possible by a doctoral fellowship from the Association Francois-Xavier Bagnoud, which is greatly appreciated. Partial support for this work was provided by Air Force Office of Scientific Research Contract Department of Defense G-F49620-95-1-0115, monitored by J. M. Tishkoff.

References

[1]Driscoll, J. F., Huh, H., Yoon, Y., and Donbar, J. M., "Measured Lengths of Supersonic Hydrogen-Air Flames—Compared to Subsonic Flame Lengths and Analysis," *Combustion and Flame*, Vol. 107, No. 1–2, 1996, pp. 176–186.

[2]Yoon, Y., Donbar, J. M., and Driscoll, J. F., "Blowout Stability Limits of a Hydrogen Jet Flame in a Supersonic, Heated, Coflowing Air Stream," *Combustion Science and Technology*, Vol. 97, No. 1–3, 1994, pp. 137–156.

[3]Huh, H., and Driscoll, J. F., "Shock-Wave-Enhancement of the Mixing and the Stability Limits of Supersonic Hydrogen-Air Flames," *Proceedings of the Combustion Institute*, Vol. 26, 1996, pp. 2933–2939.

[4]Yoon, Y., Donbar, J., Huh, H., and Driscoll, J. F., "Measured Supersonic Flame Properties: Heat-Release Patterns, Pressure Losses, Thermal Choking Limits," *Journal of Propulsion and Power*, Vol. 12, No. 4, 1996, pp. 718–723.

[5]Huh, H., "An Experimental Study of Supersonic Hydrogen-Air Flames for Scramjet Applications," Ph.D. Dissertation, Dept. of Aerospace Engineering, Univ. of Michigan, Ann Arbor, MI, Oct. 1996.

[6]Roy, C. J., and Edwards, J. R., "Numerical Simulation of a Three-Dimensional Flame/Shock Wave Interaction," *AIAA Journal*, Vol. 38, No. 5, May 2000, pp. 745–754.

[7]Masuya, G., Uemoto, T., Wakana, Y., Kudou, K., Murakami, A., and Komuro, T., "Performance Evaluation of Scramjet Combustors Using Kinetic Energy and Combustion Efficiency," *Journal of Propulsion and Power*, Vol. 15, No. 1, 1999, pp. 401–407.

[8]Chinzei, N., Komuro, T., Kudou, K., Murakami, A., Tani, K., Masuya, G., and Wakamatsu, Y., "Effects of Injector Geometry on Scramjet Combustor Performance," *Journal of Propulsion and Power*, Vol. 9, No. 1, 1993, pp. 146–152.

[9]Masuya, G., Komuro, T., Murakami, A., Shinozaki, A., Nakamura, A., Murayama, M., and Ohwaki, K., "Ignition and Combustion Performance of Scramjet Combustors with Fuel Injector Struts," *Journal of Propulsion and Power*, Vol. 11, No. 2, 1995, pp. 301–307.

[10]Eklund, D. R., Drummond, J. P., and Hassan, H. A., "Calculation of Supersonic Turbulent Reacting Coaxial Jets," *AIAA Journal*, Vol. 28, No. 9, 1990, pp. 1633–1641.

[11]Villasenor, R., Chen, J. -Y., and Pitz, R. W., "Modeling Ideally Expanded Supersonic Turbulent Jet Flows with Nonpremixed H_2-Air Combustion," *AIAA Journal*, Vol. 30, No. 2, 1992, pp. 395–402.

[12]Zheng, L. L., and Bray, K. N. C., "The Application of New Combustion and Turbulence Models to H_2-Air Non-Premixed Supersonic Combustion," *Combustion and Flame*, Vol. 99, No. 2, 1994, pp. 215–281.

[13]Baurle, R. A., Alexopoulos, G. A., and Hassan, H. A., "Assumed Joint Probability Density Function Approach for Supersonic Turbulent Combustion," *Journal of Propulsion and Power*, Vol. 10, No. 4, 1994, pp. 473–485.

[14]Heiser, W. H., and Pratt, D. T., *Hypersonic Airbreathing Propulsion*, edited by J. S. Przemieniecki, AIAA Education Series, AIAA, Washington, DC, 1994, p. 331.

[15]Cheng, T. S., Wehrmeyer, J. A., Pitz, R.W., Jarrett, O. Jr., and Northam, G. B., "Raman Measurement of Mixing and Finite-Rate Chemistry in a Supersonic Hydrogen-Air Diffusion Flame," *Combustion and Flame*, Vol. 99, No. 1, 1994, pp. 157–173.

[16]Segal, C., McDaniel, J. C., Whitehurst, R. B., and Krauss, R. H., "Mixing and Chemical Kinetics Interactions in a Mach 2 Reacting Flow," *Journal of Propulsion and Power*, Vol. 11, No. 2, 1995, pp. 308–314.

[17]Barlow, R. S., Fourguette, D. C., Mungal, M. G., and Dibble, R. W., "Experiments on the Structure of an Annular Compressible Reacting Shear-Layer," *AIAA Journal*, Vol. 30, No. 9, 1992, pp. 2244–2251.

[18]Hinze, J. O., *Turbulence*, McGraw–Hill, New York, 1959, p. 522.

[19]Papamoschou, D., and Roshko, A., "The Compressible Turbulent Shear-Layer—An Experimental Study," *Journal of Fluid Mechanics*, Vol. 197, Dec. 1988, pp. 453–477.

[20]Driscoll, J. F., Chen, R.-H., and Yoon, Y., "Nitric Oxide Levels of Turbulent Jet Diffusion Flames: Effects of Residence Time and Damkohler Number," *Combustion and Flame*, Vol. 88, No. 1, 1992, pp. 37–49.

[21]Lozano, A., Yip, B., and Hanson, R. K., "Acetone: a Tracer for Concentration Measurements in Gaseous Flows by Planar Laser-Induced Fluorescence," *Experiments in Fluids*, 13, 1992, pp. 369–376.

[22]Thurber, M. C., Grisch, F., Kirby, B. J., Votsmeier, M., and Hanson, R. K., "Measurements and Modeling of Acetone LIF with Implications for Temperature Imaging Diagnostics," *Applied Optics*, Vol. 37, No. 21, 1998, pp. 4963–4978.

[23]Bryant, R. A., Donbar, J. M., and Driscoll, J. F., "Acetone Laser Induced Fluorescence for Low Pressure/Low Temperature Flow Visualization," *Experiments in Fluids*, Vol. 28, 2000, pp. 471–476.